Received: 17 August 2023 | Revised: 22 November 2023 | Accepted: 27 November 2023

DOI: 10.1002/app.55040

RESEARCH ARTICLE

Applied Polymer SCIENCE WILEY

Effect of the filler morphology on the crystallization behavior and dielectric properties of the polyvinylidene fluoride-based composite

Suzana Filipović[1] | **Nina Obradović**[1] | **Cole Corlett**[2] | **William G. Fahrenholtz**[2] | **Martin Rosenschon**[3] | **Ekkehard Füglein**[3] | **Radovan Dojčilović**[4] | **Dragana Tošić**[4] | **Jovana Petrović**[5] | **Antonije Đorđević**[5,6] | **Branislav Vlahović**[7] | **Vladimir B. Pavlović**[8]

[1]Institute of Technical Sciences of SASA, Belgrade, Serbia

[2]Materials Science and Engineering, Missouri University of Science and Technology, Rolla, Missouri, United States

[3]NETZSCH-Gerätebau GmbH, Selb, Germany

[4]Vinča Institute of Nuclear Sciences, National Institute of the Republic of Serbia, University of Belgrade, Belgrade, Serbia

[5]School of Electrical Engineering, University of Belgrade, Belgrade, Serbia

[6]Serbian Academy of Sciences and Arts, Belgrade, Serbia

[7]North Carolina Central University, Durham, North Carolina, USA

[8]Faculty of Agriculture, University of Belgrade, Belgrade, Serbia

Correspondence
Suzana Filipović, Institute of Technical Sciences of SASA, Kneza Mihajla 35/IV, Belgrade, Serbia.
Email: suzana.filipovic@itn.sanu.ac.rs

Funding information
Ministarstvo Prosvete, Nauke i Tehnološkog Razvoja, Grant/Award Numbers: 451-03-47/2023-01/200175, 451-03-47/2023-01/200116, 451-03-47/2023-01/200103; Serbian Academy of Sciences and Arts, Grant/Award Number: F133; University of North Carolina, Grant/Award Numbers: NSF DMR EiR 2101041, NSF DMR PREM 2122044, DOE/NNSA NA0003979, USA NSF PREM award DMR 11523617

Abstract

Ceramic/polymer composites can be chemically stable, mechanically strong, and flexible, which make them candidates for electric devices, such as pressure or temperature sensors, energy storage or harvesting devices, actuators, and so forth. Depending on the application, various electrical properties are of importance. Polymers usually have low dielectric permittivity, but increased dielectric permittivity can be achieved by the addition of the ceramic fillers with high dielectric constant. With the aim to enhance dielectric properties of the composite without loss of flexibility, 5 wt% of $BaTiO_3$-Fe_2O_3 powder was added into a polyvinylidene fluoride matrix. The powder was prepared by different synthesis conditions to produce core/shell structures. The effect of the phase composition and morphology of the $BaTiO_3$-Fe_2O_3 core/shell filler on the structure and lattice dynamics of the polymer composites was investigated. Based on the results of the thermal analysis, various parameters of ceramic/polymer composites were determined. Differences in the phase composition and morphology of the filler have an influence on the formation of various polyvinylidene fluoride allomorphs and the degree of crystallinity. Furthermore, the dielectric performances of pure polyvinylidene fluoride and the polymer/ceramic composites were measured.

KEYWORDS

composites, copolymers, crystallization, dielectric properties, differential scanning calorimetry (DSC), spectroscopy

[Correction added on February 1, 2024, after print and online publication: Corresponding author details has been included]

1 | INTRODUCTION

Polymer-based dielectric materials have great potential for use in electronic devices because they possess a combination of flexibility, low loss, low weight, high breakdown strength, mechanical strength, and low processing cost.[1,2] Some of the potential applications of these materials are for sensors and actuators due to their fast electromechanical response. Polyvinylidene fluoride (PVDF)-based polymers are especially interesting due to their good chemical stability and ferroelectric characteristic.[3] The ferroelectric property depends on PVDF semicrystalline modifications. PVDF exhibits five dominant polymorphs, α, β, γ, δ, and ε, with each polymorph having distinct chain orientation during crystallization.[4] Therefore, the processing conditions strongly affect which phase is formed. Thermodynamically, the most stable polymorph is α-PVDF, which is usually obtained by cooling from melt or by solvent casting.[5,6] It is a nonpolar and nonelectroactive phase and, consequently, is less attractive for electronic applications. The β- and γ-PVDF phases possess piezo-, ferro-, and pyroelectric properties, and are, therefore, more interesting. These phases are more difficult to obtain because they are not thermodynamically stable. These variations can be formed by electrospinning or starching.[4,7,8]

The formation of the electroactive phases of the PVDF can be triggered by addition of filler particles, which act as nucleation sites for PVDF crystallization.[5] Smaller particles are more effective at promoting crystallization of the electroactive PVDF phases.[9] Mechanically activated fillers appear to induce β and γ phase formation, not only due to the reduction of particle size and increased specific surface area, but also due to their surface activity and increased defect concentration.[10,11] Further, surface modification of filler particles has been used to tailor crystallization direction. The modification of the filler surface can also improve interface compatibility between inorganic particles and organic matrix.[12,13] Addition of the ceramic filler not only affects crystallization behavior, but also increases PVDF dielectric permittivity.[1,14–18] Increasing the permittivity usually requires more than 20 vol% of ceramic filler, but such large contents have detrimental effects on flexibility.[15–20] The most frequently used ceramic filler is $BaTiO_3$ (BT) due to its high permittivity and ferroelectric properties.[11,21] More recent studies have focused on the addition of multiferroics due to their combinations of attractive properties.[22,23] Thin film multiferroics are compounds in which electric, magnetic, and piezo order states coexist within the material and generate magnetoelectric (ME) strain. The resulting combinations of properties can lead to applications such as microsensors, microelectromechanical systems (MEMS) devices, and high-density information storage.[24] Multiferroic composites as fillers in the PVDF matrix are still an attractive area of research. Activation of ME strain can influence phase formation and microstructure development, but may also influence the final magnetic and dielectric properties. In the three components multiferroic polymer composite, shear flow, magnetic field, electric field, or electric force can change the molecular arrangement of a polymer and the distribution of conductive particles in a host polymer, which influence the microstructure and macroproperties of composites.[23,25] When the electric or magnetic field is applied to the composite film, dipoles or spins align along the direction of the external field. Electric domain walls and chain move accordingly, leading to strain formation. If the ferroelectric and ferromagnetic phases are well coupled, this strain of the PVDF matrix and magnetic shell results in BT core dipole orientation, accumulation of the charges at the surfaces of the constituents, and leads to change in dielectric properties.[26]

Hence, in this paper, the effect of phase composition and morphology of the multiferroic filler, synthesized at various conditions, on semicrystalline modification, stability, and dielectric properties of the PVDF-based thin films is investigated.

2 | METHODS

The procedure for powder synthesis was reported previously.[27] Briefly, filler powders denoted as BTF1 and BTF2 were prepared by sonication-assisted precipitation at pH = 12. The BT (Sigma Aldrich, Germany) to Fe_2O_3 (synthesized from $Fe(NO_3)_3{\cdot}9H_2O$ [Sigma Aldrich, Germany] and NaOH [Sigma Aldrich, Germany]) mass ratios were 1.2 and 0.8, respectively. Samples BTF3 and BTF4 were precipitated at pH = 6, with BT to Fe_2O_3 mass ratios of 1.2 and 0.8, respectively. The BTF1-BTF4 powders were subsequently heated in a furnace at 300°C for 1 h to promote formation of the iron oxide phase. The powder BTF5 was precipitated at pH = 9, with a BT to Fe_2O_3 mass ratio of 1.2, and additionally heated at 500°C for an hour.

The BTF/PVDF-HFP composites were prepared by the solution casting method. A stock solution containing 10 vol% of a poly(vinylidene fluoride-*co*-hexafluoropropylene) (PVDF-HFP) copolymer (Sigma-Aldrich, Saint

Louis, USA, Mw ~455,000) denoted PVDF-HFP was prepared by dissolution of the 10 g of polymer in 100 mL of *N*,*N*–dimethylformamide (DMF, Sigma Aldrich, Saint Louis, USA). BTF1-BTF5 powders (50 mg) were dispersed in 10 mL of DMF and sonicated in a Branson W-450 D Digital Sonifier for 10 min at 20% amplitude (80 W). The obtained dispersion was mixed with the PVDF-HFP solution to obtain the composites with 5 wt% of inorganic content. In addition, the polymer composites with the 10 wt% were also made, but due to lower flexibility of those, we proceeded with the investigation of the composites made with 5 wt% of the filler. Dispersions were mixed with a magnetic stirrer for 10 min, cast into glass Petri dishes, and dried at 100°C for 10 h to evaporate the solvent. Pure PVDF-HFP film was prepared using the same procedure, but without adding the powders.

Transmission electron microscopes (TEM) images of the ceramic fillers were collected by JEM-1400 (120 kV) equipment. Samples were prepared by sonication of 0.5 mg dry powders in 1 mL of ethanol for 2 h. Suspensions were deposited onto carbons meshes. Grain size was determined from image analysis (ImageJ) by counting at least 50 grains.

Phase composition of the composite films was analyzed by x-ray diffraction (XRD, PANalytical X-Pert Pro, Malvern Panalytical Ltd., Royston, UK) in the 2θ range of 5°–90°, at ambient conditions. Fourier transform infrared (FT-IR) spectra were recorded on a Thermo Scientifc™ Nicolet™ iS™10 FT-IR spectrometer equipped with attenuated total reflectance (ATR) accessory. The ATR/FT-IR measurements were done in the wavenumber region of 400–4000 cm^{-1}, with a resolution of 4 cm^{-1}. SEM/EDS were done on Helios Nanolab 600 FIB/SEM (FIB is defined as focused ion beam) equipped with energy-dispersive spectroscopy. Differential scanning calorimetry was performed using a NETZSCH differential scanning calorimetry (DSC) 214 *Polyma*, with a heating rate 10°C/min in an aluminum pan with pierced lid. The purge gas was N_2 at a flow rate of 40 mL/min. Thermal gravimetric analysis was conducted on a NETZSCH TG 209 *F1 Libra*® (TG is defined as Thermogravimetric) with the same heating rate. The gas atmosphere was as follows: from room temperature (RT) to 800°C N_2 with flowing rate of 40 mL/min and from 800 to 1000°C synthetic air mixture was used (20/80 O_2/N_2) and flowing rate of 40 mL/min. The measurements were done in temperature range from RT to 1000°C in an Al_2O_3 crucible.

The dielectric parameters (relative permittivity and loss tangent) were estimated from the reflection-coefficient measurements of a custom-made coaxial chamber with a disk-shaped specimen.[28] Measurements were performed in the frequency range from 50 Hz to 500 kHz using an Inductance (L), Capacitance (C), and Resistance (R) (LCR) meter (Microtest 6366), while a vector network analyzer (Agilent E5061A) was used for the measurements in the frequency range from 500 kHz to 300 MHz. In order to extract the dielectric parameters of the specimens, the experimentally obtained data were compared with the results of electromagnetic analysis using a numerical model of the chamber. The reflection coefficient of the numerical model was calculated for various dielectric parameters of the sample. The extracted dielectric parameters were those that provided the closest match between the measured and calculated reflection coefficients.

3 | RESULTS AND DISCUSSION

Morphology of the composite materials changes with synthesis conditions as shown in Figure 1. The sample produced at pH = 12 and with a BT to Fe_2O_3 ratio of 1:1.2 had needle-like particles of the Fe-phases 290 ± 50 nm in length, surrounding larger, polygonal BT particles (Figure 1a). The Fe-rich and BT phases appear to be separate, distinct particles in this specimen. Other samples are characterized by rounded iron oxides particles forming shells over larger BT particles. Due to ultrasound-assisted synthesis, the individual particles of the BT were seen. The BTF3 specimen shows the best coverage among micrographs presented in Figure 1. The iron oxide particles appear to be the smallest, 5.0 ± 1.9 nm. For the samples denoted BTF3-BTF5, agglomerates of the starting BT particles were noticed. Hence, BT agglomerates were covered by spherical iron-based particles; individual BT grains are highlighted in Figure 1c. Poorer coverage of the iron oxide phase was observed for samples BTF4 and BTF5 and the larger particles size of 11 ± 2.6 and 17 ± 7 nm, respectively. Although the full covering is not achieved, the core/shell structure is observed. Lower pH values and higher BT to Fe_2O_3 mass ratios seem to have a beneficial effect on the morphology and coupling between phases.

XRD patterns for pure PVDF and PVDF/BTF1-BTF5 are shown in Figure 2. The patterns show reflections of the BT and PVDF phases. Strong and narrow reflections in the patterns originate from highly crystalline BT (075–2119 JCPDS card of BT). Asymmetric appearance of the peak at 2θ of 45° indicates that tetragonal BT was present.[29] The peaks of the iron oxide were not observed in the XRD patterns due to the low amount in the composite samples and its nanosized dimensions.[27,30] In addition, the main peaks of the α-Fe_2O_3 should be observed at 33° and 35°, but are be covered by broad peaks of PVDF in that region. Even pure α-Fe_2O_3 synthesized at 700°C shows low intensity of XRD peaks.[31]

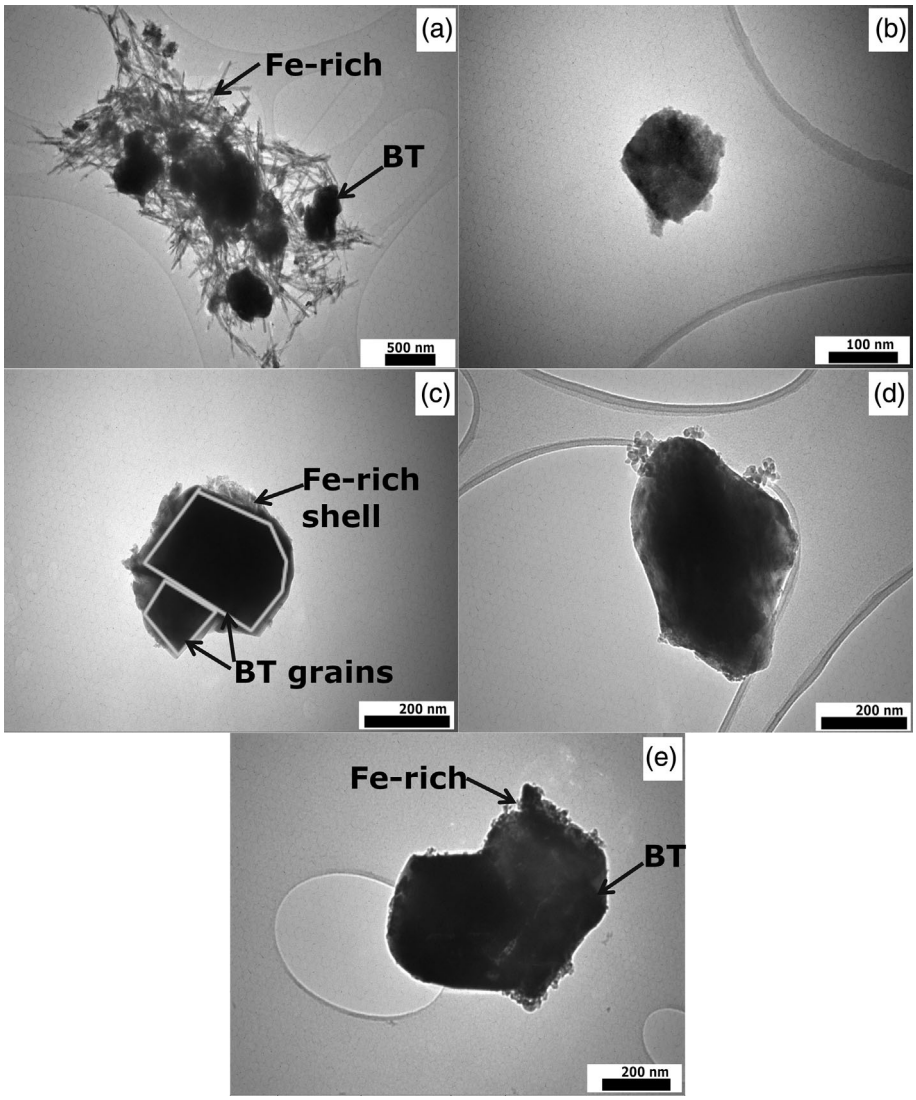

FIGURE 1 TEM images of the filler powders showing (a) BTF1; (b) BTF2; (c) BTF3; (d) BTF4; and (e) BTF5. Note that the magnification varies among the images. BT, $BaTiO_3$.

Appearance of the broad and low intensity peaks is characteristic of PVDF since the crystalline content typically does not exceed 60%.[4] The pure PVDF sample appears to be mixture of β-PVDF and γ-PVDF. The β-PVDF phase is characterized by strong peak at 20.3° from the (110) and (200) planes, while a weak peak from the (020) plane was observed at 36.3°.[9,10] Peaks at $2\theta = 18.5°$ and 20.2° dominate in the γ-PVDF, but also appear in the α-PVDF polymorph. Since the peak at 39.0° is not present in the monoclinic polymorph, peaks at 18.5° and 20.2° were attributed to γ-PVDF.[4] When the PVDF is dissolved in polar solvents and crystallization occurs at RT, dipole molecules at the surface of the droplets are oriented perpendicularly to the interface, and interactions on the surfaces lead to all-trans planar configurations (characteristic of the β-PVDF phase) of the CH_2–CH_2 dipoles.[32]

The XRD pattern of the sample denoted as PVDF/BTF1 shows peaks consistent with β-PVDF phase, while the composites PVDF/BTF2 and PVDF/BTF3 are consistent with mixtures of β-PVDF and γ-PVDF, based on the appearance of peaks at 18.5°, 20.3°, and broad peaks with low intensity at 36.3° and 39.0°. Because of the polarity of OH groups at the surface of the multiferroic composites (Fe_2O_3@BT), interactions were stronger at interfaces between Fe_2O_3@BT nanoparticles and PVDF, leading to local orientation of CH_2–CF_2 dipoles that are packed in the *trans* configuration.[32] Existence of the strain induced by multiferroic coupling can strongly influence the orientation of the PVDF dipoles in the appropriate direction.

In PVDF/BTF4 and PVDF/BTF5, incorporation of the core/shell Fe_2O_3@BT particles triggers formation of monoclinic PVDF.[33] Besides interactions that occur at the interfaces that determine chains orientation during crystallization, the filler size also plays important role. For the bigger particles, the specific surface area available for O-H bonding decreases, and thus crystallization of α-PVDF was favorable.[32] For BTF4 and BTF5, the agglomerates were covered with Fe_2O_3 (Figure 1d,e), which increased overall filler particle size and led to α-PVDF formation. From the application point of view,

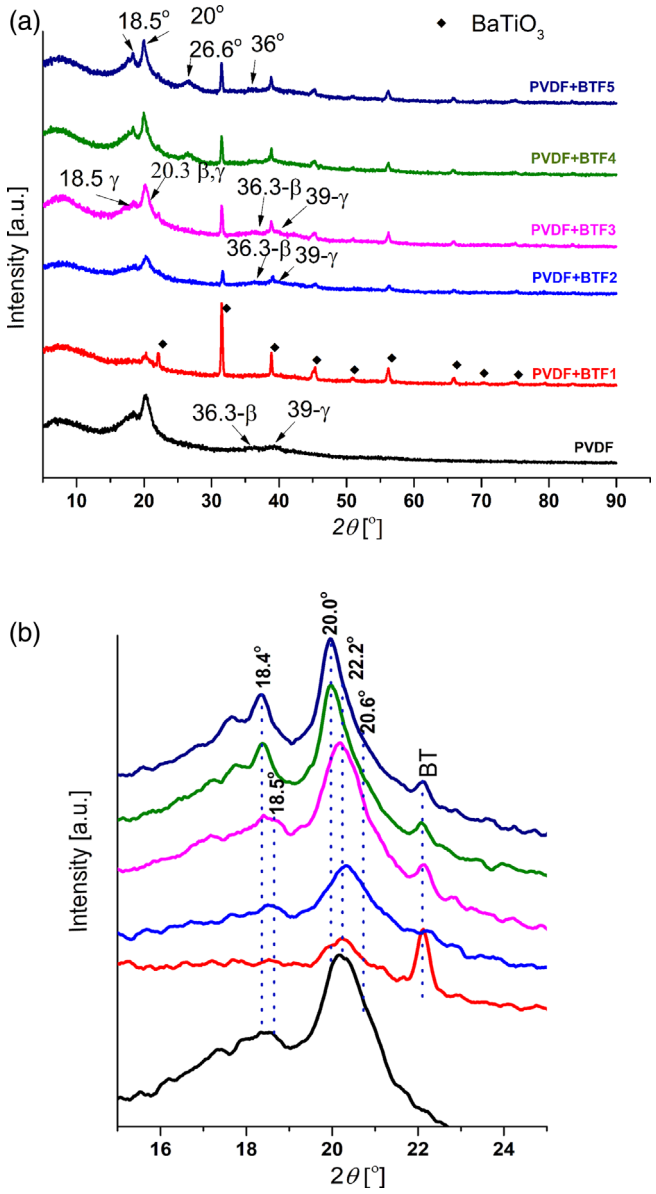

FIGURE 2 X-ray diffraction patterns of the polyvinylidene fluoride (PVDF) and the samples PVDF/BTF1-BTF5, (a) 2θ range 5–90 and (b) magnified 2θ range 15°–25°. [Color figure can be viewed at wileyonlinelibrary.com]

β-PVDF and γ-PVDF are ferroelectric and hence interesting for use in materials for electronic components, while α-PVDF is nonpolar and not electroactive and hence not as attractive for such applications.[10,33]

The FT-IR spectrum of pure PVDF (Figure 3) showed all of the dominant peaks of the PVDF phases were detected. Characteristic peaks shared by α-, β- and γ-PVDF were detected at 877, 1070, 1167, and 1042 cm^{-1}, which make it difficult to determine the specific PVDF phases present. However, shoulders on the main peaks at 1275 and 1431 cm^{-1} are exclusive for β-phase. In addition, peaks at 1234, 774, and 483 cm^{-1} imply the presence of the γ-phase. Furthermore, two strong peaks were

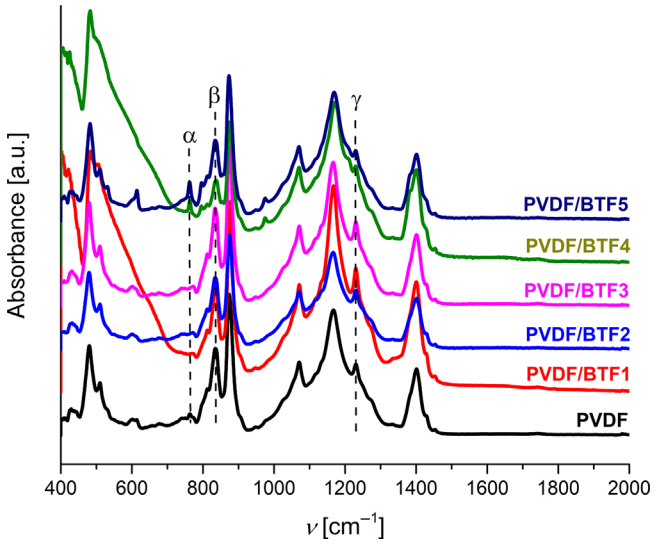

FIGURE 3 Fourier transform infrared spectra of the pure polyvinylidene fluoride (PVDF) and PVDF mixed with 5 wt% BTF1-BTF5. [Color figure can be viewed at wileyonlinelibrary.com]

observed at ~840 and ~510 cm^{-1}. Although these peaks occur in the α-phase, they can be used for identification of β- and γ-phases because these phases have stronger absorbance at these frequencies than the α-phase.[4] Based on the stronger lines associated with the γ-phase, the pure PVDF contains a mixture of β- and γ-phases, which is consistent with the XRD results.

The spectra of PVDF/BTF1, PVDF/BTF2, and PVDF/BTF3 show an increase in intensity at 1234 cm^{-1}, which is characteristic for the γ-phase. On the other hand, PVDF/BTF4 and PVDF/BTF5 have modes at 764 and 974 cm^{-1}, which are characteristic of the α-phase. The significant increase of the 764 and 974 cm^{-1} modes combined with a decrease of the mode at 1234 cm^{-1} indicates transformation from the γ- to the α-PVDF polymorph. The presence of the mode 840 and 1275 cm^{-1} in all samples indicates the coexistence of the β-phase with the other detected PVDF phases. Overall, analysis of XRD and FT-IR data shows that fillers induce transformation from γ- to α-PVDF polymorph, while β-PVDF is present in all PVDF/BTF compositions.

The fraction of β-PVDF phase present in each sample was calculated using procedure explained by Gregorio and Cestari[34] and Salimi and Yousefi[8] For each phase present in the polymer, the Equation (1) stands as follows:

$$A = \log \frac{I^{o}}{I} = \varepsilon X L, \tag{1}$$

where A is absorbance and I^{o} and I are incident and transmitted radiation intensities, respectively. L is film thickness, X is degree of crystallinity of phases, and ε is the excitation coefficient of IR bands corresponding to

TABLE 1 Results of the relative fraction of the β-PVDF phase calculation.

Sample	$F(\alpha)$ (%)	$F(\beta)$ (%)	$F(\gamma)$ (%)
PVDF	3	79	18
PVDF/BTF1	0	67	33
PVDF/BTF2	6	69	25
PVDF/BTF3	3	71	26
PVDF/BTF4	17	66	17
PVDF/BTF5	24	67	9

Abbreviation: PVDF, polyvinylidene fluoride.

each phase. For the calculations of the relative fraction of β-PVDF phase previously determined the $K_\alpha = 6.1 \times 10^4$, $K_\beta = 7.7 \times 10^4$, $K_\gamma = 5.8 \times 10^4\,\mathrm{cm^2/mol}$ were used.[8,34] Applying Lamnert–Beer low for the samples with more than one semicrystalline phase, the equation for calculation relative fraction of the β-PVDF phase ($F(\beta)$) is given by Equation (2):

$$F(\beta) = \frac{X_\beta}{X_\alpha + X_\beta + X_\gamma}. \quad (2)$$

Replacing Equation (1) in Equation (2), the $F(\beta)$ can be calculated by Equation (3):

$$F(\beta) = \frac{A_\beta}{\frac{K_\beta}{K_\alpha}A_\alpha + A_\beta + \frac{K_\beta}{K_\gamma}A_\gamma}. \quad (3)$$

For the calculation, the integral area of the specific modes for each phase was used. As the majority of the modes are common in PVDF for all three semicrystalline phases, the modes at 763, 840, and 1234 $\mathrm{cm^{-1}}$ for α-, β-, and γ-phase, respectively, were chosen. The results were summarized in Table 1.

As can be noted, the percentage of β-PVDF did not changed significantly. The highest value, among ceramic/polymer composites, was assigned to PVDF/BTF3 sample. The increase in percentage of γ-PVDF was more pronounced. An addition of the multiferroic composites BTF1-BTF3 promotes formation of the γ-phase, while the fillers BTF4 and BTF5 favor crystallization of the PVDF in α-phase.

The microstructure of the composites was investigated by SEM as shown in Figure 4, with labels indicating points where energy dispersive spectroscopy (EDS) analysis was performed. Pure PVDF had a smooth surface, which indicated that the film was uniformly cast. Ceramic particles were visible as bright spots on the surface and appeared to be well distributed within the polymer matrix for the PVDF-BTF compositions. The preparation conditions whereby the inorganic component were well-dispersed in DMF before mixing with the PVDF solution promoted uniform distribution of the filler. Some examples of powder aggregation were observed, but the polymer matrix remained smooth and consistent. No significant changes in microstructure were observed among the films with different ceramic additives. To further confirm the compositions of the filler and polymer matrix, EDS analysis was performed. EDS spectra of the bright spots show the presence of the Ba, Ti, Fe, and O, and EDS of the bulk shows majority of the F originates from the PVDF matrix. Table 2 summarizes the compositions at the points shown in Figure 4.

Filler additions affect the melting enthalpy in both the first and second heating cycles as well as the crystallization in the cooling segment, as shown in Figure 5. Degree of crystallinity (χ_c), calculated by Equation (4)[35,36] and by using enthalpy of the first heating cycles, is summarized in Table 3.

$$\chi_c = \frac{\Delta H_m}{(1-\omega)\Delta H_m^0} 100\%, \quad (4)$$

where ΔH_m is the measured melting enthalpy of the PVDF and PVDF-BTF samples, ΔH_m^0 is the melting enthalpy of the fully crystallized P(VDF-HFP) polymer, which is 104.6 J/g,[5] and ω is the weight fraction of Fe_2O_3@BT particles in the polymer composites.

A slight decrease in the peak temperature for the melting process was observed for the second heating cycle for all compositions. Two possible reasons could explain the change, which are (1) a decrease in crystallinity after the crystallization from the melt after first heating cycle and (2) improved sample to crucible contact in the second cycle after the sample was molten during the first cycle.[37] Lower crystallinity was observed previously for melt synthesized PVDF films.[38] For solvent cast films, the slow evaporation of the solvent allows rearrangement of the polymer chains and increases overall crystallinity compared with melt casting.[37]

Crystallization curves for PVDF/BTF1 and PVDF/BTF2 exhibited multiple peaks (example of the PVDF/BTF1 is given in Figure 5b) (DSC curves for the samples PVDF/BTF2-PVDF/BTF5 were given in Supplementary S1). This behavior could be due to the crystallization rate and/or the crystallization of multiple PVDF polymorphs catalyzed most likely due to presence of various phases in the BTF1 and BTF2 ceramic powders, as shown in our previous paper.[27] The FeO(OH), that is present in these two filler, according to XRD published previously,[27] could induce linking with PVDF chains in various orientations trough formation of hydrogen bonding.

The degree of crystallinity decreases with filler additions from 67% for pure PVDF to 61% for PVDF/BTF1. The submicron Fe_2O_3@BT particles retard the

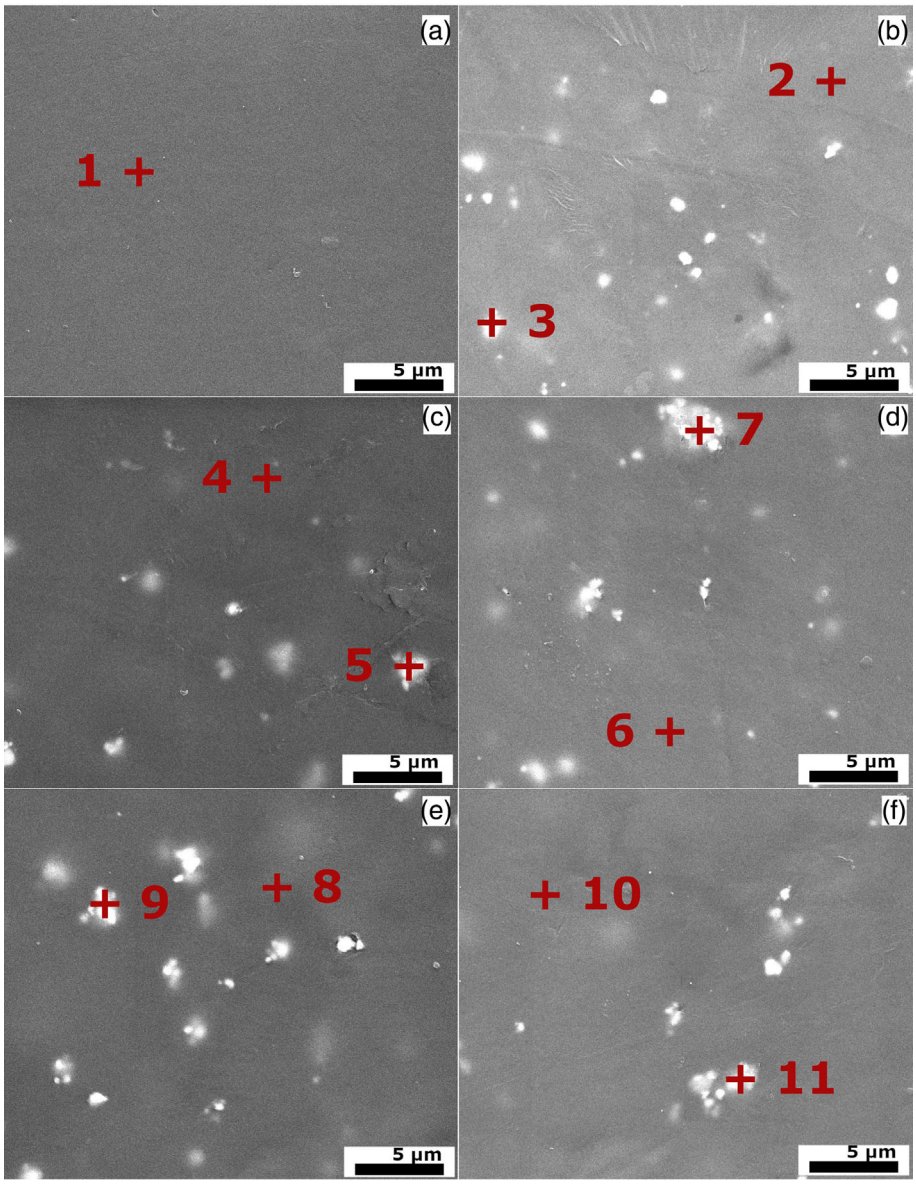

FIGURE 4 Microstructure of the pure polyvinylidene fluoride (PVDF) and PVDF with fillers, (a) PVDF, (b) PVDF/BTF1, (c) PVDF/BTF2, (d) PVDF/BTF3, (e) PVDF/BTF4, and (f) PVDF/BTF5. [Color figure can be viewed at wileyonlinelibrary.com]

movement of the polymer chains and impede the progress of crystallization.[35] Higher degrees of crystallinity were observed for PVDF/BTF2 and PVDF/BTF3, which were above 65%. The filler in PVDF/BTF3 was previously shown to increase the ME coupling between the BT and iron oxide.[27,30] Strain formed by ME coupling within the filler could increase crystallization in the electroactive β- and γ-PVDF phases as well as the overall crystallization of the PVDF/BTF3 composites.[39,40] Moreover, the ceramic filler was mainly homogeneously distributed in the composites (Figure 4), but aggregation was present, which could also influence the local crystallization. Hence, the choice of the location for extracting the DSC sample could also influence the results for degree of crystallinity. Finally, all samples in the present study had a higher degree of crystallinity than is usually reported.[4,21,35,41]

The thermal stability of the PVDF and the PVDF/BTF composites is shown in Figure 6. Mass loss occurs in two stages. The first stage occurs around 400°C and is accompanied with the mass loss of 69% for pure PVDF and 65% for the composites with the filler. The second stage is above 800°C and leads to complete decomposition. Ceramic filler additions shift the onset of the degradation to higher temperatures, from 424°C for the pure PVDF, to around 435°C for the composites, indicating more stable systems. Furthermore, pure PVDF had the highest mass loss, indicating complete decomposition by 1000°C. For the composites with fillers, the residual mass after heating to 1000°C was due to the added ceramic. The first step was pyrolysis and was conducted in nitrogen. For pure PVDF, ∼30 wt% of pyrolytic carbon was produced in the first stage of the mass loss, which then burned at higher temperatures when the atmosphere was switched

TABLE 2 Results of the EDS analysis.

Sample	Point	Elements (wt%)				
		F	Ba	Ti	O	Fe
PVDF	1	99.1	0.3	0.3	0.3	0.0
PVDF/BTF1	2	90.2	7.0	0.8	0.8	1.2
	3	52.6	28.9	10.1	7.9	0.5
PVDF/BTF2	4	99.3	0.2	0.2	0.0	0.3
	5	67.9	17.9	6.5	4.8	2.9
PVDF/BTF3	6	93.8	4.1	1.8	0.0	0.3
	7	53.0	22.0	13.7	8.5	2.7
PVDF/BTF4	8	94.3	2.7	1.4	1.4	0.2
	9	40.7	37.9	11.9	9.0	0.6
PVDF/BTF5	10	85.4	10.6	2.3	1.1	0.7
	11	58.6	15.7	15.3	5.7	4.7

Abbreviation: PVDF, polyvinylidene fluoride.

to air. For all filled samples, the first step mass loss was smaller due to the lower polymer content and the residual mass was higher due to the inorganic residue.

The relative permittivities (ε_r, dielectric constant) and loss tangents of pure PVDF and the PVDF/BTF composites are shown in Figure 7. At lower frequencies, ε_r has higher values, which decrease as the frequency of the applied field increases. The decrease is due to dipole and space charged relaxations in this frequency range.[2,23] The relative dielectric permittivity in the PVDF originates from the strong dipole moment due to electronegative fluorine atoms in the molecular structure.[42] With exception of PVDF/BTF1, all composites have higher ε_r values than pure PVDF due to the space-charge effect. The presence of filler particles in the composites produced more surfaces for charges to accumulate. Generally, the permittivity values could be divided into two groups. The first group comprises PVDF, PVDF/BTF1, and PVDF/BTF2, which has lower ε_r values (around 3 at 10^5 Hz). The second group is PVDF/BTF3, PVDF/BTF4, and PVDF/BTF5 with ε_r values above 5 at 10^5 Hz, which are nearly two times those of the first group. The higher ε_r values of group 2 are due to higher BT content of the ceramic filler in those compositions. BT ceramics have high dielectric constant, around 2000–3000, depending on particle size, agglomeration, and so forth. Based on XRD results, the powders BTF3-BTF5 have estimated BT content of 90–95 wt% of the ceramic filler, while in the powders BTF1 and BTF2, the BT content is 50–63 wt% of the filler.[27] Thus, the observed trend in ε_r can be explained by the rule of mixtures. The highest dielectric constant is expected for PVDF/BTF4, which has BT content of 95 wt % of the filler. However, the highest ε_r was measured for the sample PVDF/BTF3. The ME coupling between

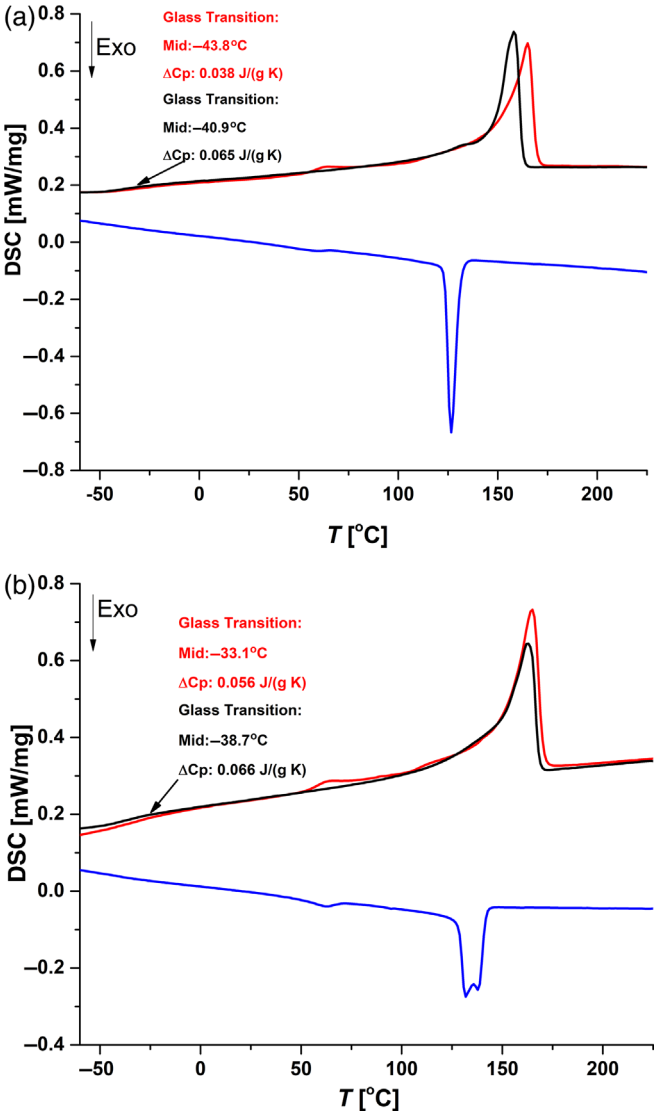

FIGURE 5 Differential scanning calorimetry (DSC) curves of (a) polyvinylidene fluoride (PVDF) and (b) PVDF/BTF1. Results are summarized in Table 1. Red line—the first heating cycle, black line—the second heating cycle, and blue line—cooling. [Color figure can be viewed at wileyonlinelibrary.com]

phases is expected to be the highest for PVDF/BTF3,[30] which could lead to an additional increase in ε_r.[35] In the case of the low amount of the filler, increase in the effective dielectric constant should be attributed to the synergetic of a high dielectric constant of the BT and also the introduction of Fe_2O_3@BT platelets can provide more interface area. The interface among the Fe_2O_3 nanoparticles, BT platelets and PVDF polymer matrix could promote the accumulation and migration of the charge carriers. Having in mind the semiconducting nature of the Fe_2O_3 nanoparticles,[43] they possess much higher conductivity than the BT or PVDF-HFP polymer matrix.[44] The difference in conductivities could induce more space charge polarization at the interface.[45] With exception of

TABLE 3 DSC parameters for PVDF and the PVDF/BTF composites.

Sample	T_m (°C)	T_c (°C)	T_m (°C)	ΔH (J/g)	ΔH (J/g)	ΔH (J/g)	χ_c (%)
	First heating	Cooling	Second heating	First heating	Cooling	Second heating	
PVDF	165.1	126.6	158.3	67.19	−59.17	59.18	67.6
PVDF/BTF1	164.8	131.8	162.5	61.18	−55.15	52.23	61.5
PVDF/BTF2	165.1	127.5	159.6	64.67	−57.26	55.83	65.1
PVDF/BTF3	164.9	128.8	158.1	65.24	−55.28	55.29	65.6
PVDF/BTF4	160.4	132.3	159	62.59	−57.10	54.27	62.9
PVDF/BTF5	160.2	129.7	158.3	62.90	−54.70	54.44	63.3

Abbreviations: DSC, differential scanning calorimetry; PVDF, polyvinylidene fluoride.

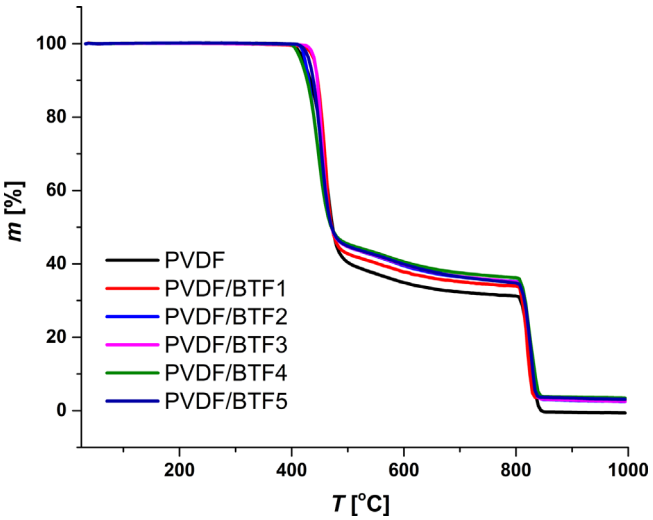

FIGURE 6 TG of the pure polyvinylidene fluoride (PVDF) and the PVDF/BTF composites. [Color figure can be viewed at wileyonlinelibrary.com]

the PVDF/BTF1composite that had weekly bonded Fe-phase to the BT particles (Figure 1), all other fillers had tight bonded iron oxide nanoparticles to the BT core, promoting the charge accumulation. Hence, the morphology and phase composition of the initial powder composite of the fillers significantly affect the dielectric properties of the final ceramic/polymer composite films.

Additionally, previous studies concluded that the PVDF crystalline phase also affects the dielectric permittivity, with α-PVDF having a higher dielectric permittivity than the β- and γ-PVDF phases.[2] The polarization appears to be increased by presence of the α- and β-interface polarization in the composites with existence of both polymorphs.[42] While other factors affect ε_r, BT content and ME coupling are the most important.

The effect of the filler on the dielectric properties of the PVDF-based films was extensively investigated. It has been shown that for notable increase in the dielectric permittivity high content of the fillers, above percolation

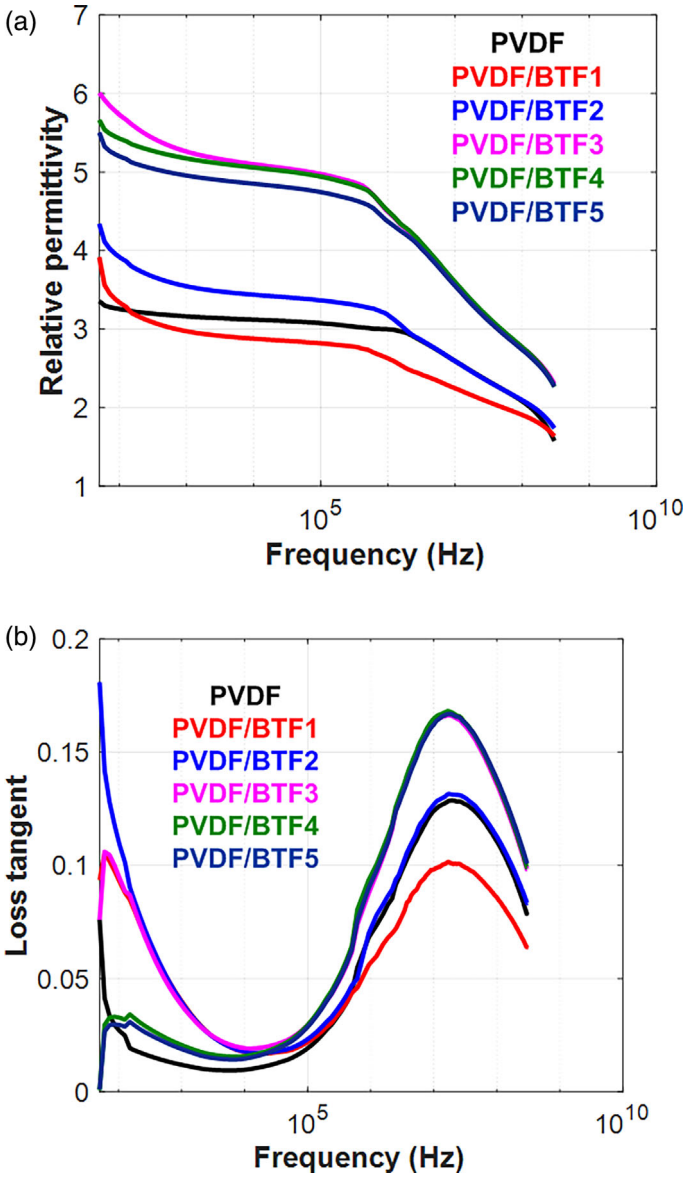

FIGURE 7 (a) Relative dielectric permittivity and (b) loss tangent of polyvinylidene fluoride (PVDF), PVDF/BTF1, PVDF/BTF2, PVDF/BTF3, PVDF/BTF4, and PVDF/BTF5. [Color figure can be viewed at wileyonlinelibrary.com]

threshold (>15 wt%), was required.[23,46] On the other hand, the attempts to enhance the dielectric properties of the PVDF-based composites with lower amount of the filler showed slight improvement. The most frequently used filler was BT. Improvement of the dielectric permittivity of 40% was observed when the 6 wt% of the mechanically activated BT was added.[11] Valuable increase in dielectric properties, for similar BT/Fe_2O_3 composite doped PVDF film, was achieved when the content of the filler was 10 wt% or more.[35] In our investigation, almost two times higher dielectric constant was measured for selected fillers (BTF3-BTF5), which was attributed to variations in phase content and morphology of the added multiferroic composites.

Figure 7b shows the loss tangent as a function of frequency for all compositions. At the beginning, the losses decrease up to 10 kHz. As the frequency increases further, the loss tangent increases and reaches a peak around 10 MHz, which is related to the dipole relaxation. Similar behavior was observed in PVDF composites filled with BT, BT/Fe_3O_4, or BT/graphite.[20,23,46] At frequencies around 100 kHz, the loss tangent reaches its minimum (below 0.02), which is slightly lower than reported for similar materials.[35] On the contrary, a significant increase in loss tangent was expected due to the incorporation of iron oxide, which is a semiconductor and would lead to charge flow through the composite. The lack of an observed increase can be explained by the choice of the iron oxide content and the morphology of the Fe_2O_3@BT particles that suppresses direct contact among the Fe_2O_3 nanoparticles. Connection of the semiconducting particles to BT retarded the formation of Fe_2O_3 networks, which inhibits charge transport.[23]

4 | CONCLUSIONS

The effects of phase composition and morphology of a multiferroic filler on the phase formation, thermal stability, and dielectric properties of the PVDF-based thin films were investigated. The filler was uniformly distributed within polymer matrix. Although some particles aggregation was present, it did not seem to affect the functional properties. The phase composition and morphology of the fillers influenced the transition from γ- to α-PVDF polymorph, while β-PVDF was present in all composites. Relative contents of all PVDF semicrystalline phases were determined from FT-IR spectra, and they confirmed transition from γ- to α-PVDF polymorph. Thermal analysis revealed a high level of crystallinity, over 60% for all samples, which decreased slightly for ceramic/polymer composites due to the hindering effect. The highest crystallinity was observed for the sample PVDF/BTF3 because of the increased ME effect of the core/shell structure of the filler. An increase of the dielectric permittivity was ascribed to synergetic contribution of the BT content and ME coupling within ceramic filler. Losses depended on frequency and type of the additive. Hence, the appropriate choice of filler content and morphology can significantly reduce dielectric losses in a chosen frequencies range.

AUTHOR CONTRIBUTIONS

Suzana Filipović: Conceptualization (equal); investigation (equal); writing – original draft (lead); writing – review and editing (equal). **Nina Obradović:** Funding acquisition (equal); investigation (equal); writing – review and editing (equal). **Cole Corlett:** Investigation (equal); writing – review and editing (equal). **William G. Fahrenholtz:** Supervision (equal); validation (lead); writing – review and editing (equal). **Martin Rosenschon:** Investigation (equal); writing – review and editing (equal). **Ekkehard Füglein:** Investigation (equal); writing – review and editing (equal). **Radovan Dojčilović:** Investigation (equal); writing – review and editing (equal). **Dragana Tošić:** Investigation (equal); writing – review and editing (equal). **Jovana Petrović:** Investigation (equal); writing – review and editing (equal). **Antonije Đorđević:** Funding acquisition (equal); investigation (equal); writing – review and editing (equal). **Branislav Vlahović:** Funding acquisition (equal); writing – review and editing (equal). **Vladimir B. Pavlović:** Funding acquisition (equal); methodology (lead); writing – review and editing (equal).

ACKNOWLEDGMENTS

This work was financially supported by the Ministry of Science, Technological Development and Innovation of the Republic of Serbia, through agreements related to the realization and financing of scientific research work at the Institute of Technical Sciences of SASA, Faculty of Agriculture of the University of Belgrade, School of Electrical Engineering of the University of Belgrade, and Vinča Institute of Nuclear Sciences, National Institute of the Republic of Serbia of the University of Belgrade in 2023 (Contract numbers, 451-03-47/2023-01/200175, 451-03-47/2023-01/200116, 451-03-47/2023-01/200103, 451-03-47/2023-01/200017), by the Serbian Academy of Sciences and Arts (Project F133) as well as the support for North Carolina Central University, award numbers, NSF DMR EiR 2101041, NSF DMR PREM 2122044, and DOE/NNSA NA0003979 and USA NSF PREM award DMR 11523617.

CONFLICT OF INTEREST STATEMENT

The authors declare no conflicts of interest.

DATA AVAILABILITY STATEMENT

The raw/processed data required to reproduce these findings cannot be shared at this time as the data also form part of an ongoing study.

ORCID

Suzana Filipović https://orcid.org/0000-0001-6383-8327

REFERENCES

[1] J.-H. Bae, S.-H. Chang, *Funct. Compos. Struct.* **2019**, *1*, 012003.
[2] W. Xia, Z. Zhang, *IET Nanodielectrics* **2018**, *1*, 17.
[3] Y. Zhang, Q. Chi, L. Liu, T. Zhang, C. Zhang, Q. Chen, X. Wang, Q. Lei, *ACS Appl. Energy Mater.* **2018**, *1*, 6320.
[4] X. Cai, T. Lei, D. Sun, L. Lin, *RSC Adv.* **2017**, *7*, 15382.
[5] A. C. Lopes, C. M. Costa, C. J. Tavares, I. C. Neves, S. Lanceros-Mendez, *J. Phys. Chem. C* **2011**, *115*, 18076.
[6] S. Satapathy, S. Pawar, P. K. Gupta, K. B. R. Varma, *Bull. Mater. Sci.* **2011**, *34*, 727.
[7] R. Ashiri, *Vib. Spectrosc.* **2013**, *66*, 24.
[8] A. Salimi, A. A. Yousefi, *Polym. Test.* **2003**, *22*, 699.
[9] V. P. Pavlović, V. B. Pavlović, B. Vlahović, D. K. Božanić, J. D. Pajović, R. Dojčilović, V. Djoković, *Phys. Scr.* **2013**, *T157*, 014006.
[10] A. Peleš, O. Aleksić, V. P. Pavlović, V. Djoković, R. Dojčilović, Z. Nikolić, F. Marinković, M. Mitrić, V. Blagojević, B. Vlahović, V. B. Pavlović, *Phys. Scr.* **2018**, *93*, 105801.
[11] T. G. Mofokeng, A. S. Luyt, V. P. Pavlović, V. B. Pavlović, D. Dudić, B. Vlahović, V. Djoković, *J. Appl. Phys.* **2014**, *115*, 084109.
[12] Z.-M. Dang, H.-Y. Wang, H.-P. Xu, *Appl. Phys. Lett.* **2006**, *89*, 112902.
[13] F. Ram, P. Kaviraj, R. Pramanik, A. Krishnan, K. Shanmuganathan, A. Arockiarajan, *J. Alloys Compd.* **2020**, *823*, 153701.
[14] S. Bonardd, A. Alegria, C. Saldias, A. Leiva, G. Kortaberria, *ACS Appl. Mater. Interfaces* **2018**, *10*, 38476.
[15] D. Yu, N. Xu, L. Hu, Q. Zhang, H. Yang, *J. Mater. Chem. C* **2015**, *3*, 4016.
[16] Y. Xie, W. Jiang, T. Fu, J. Liu, Z. Zhang, S. Wang, *ACS Appl. Mater. Interfaces* **2018**, *10*, 29038.
[17] Y. Zhou, H. Wang, *Appl. Phys. Lett.* **2013**, *102*, 132901.
[18] J.-K. Yuan, Z.-M. Dang, S.-H. Yao, J.-W. Zha, T. Zhou, S.-T. Li, J. Bai, *J. Mater. Chem.* **2010**, *20*, 2441.
[19] J. Fu, Y. Hou, M. Zheng, Q. Wei, M. Zhu, H. Yan, *ACS Appl. Mater. Interfaces* **2015**, *7*, 24480.
[20] Y. C. Li, S. C. Tjong, R. K. Y. Li, *eXPRESS Polym. Lett.* **2011**, *5*, 526.
[21] F. A. Sánchez, M. Redondo, J. González-Benito, *J. Appl. Polym. Sci.* **2015**, *132*, 41497. https://doi.org/10.1002/app.41497
[22] C. Behera, R. N. P. Choudhary, P. R. Das, *J. Mater. Sci.: Mater. Electron.* **2017**, *28*, 2586.
[23] C. Zhang, Q. Chi, J. Dong, Y. Cui, X. Wang, L. Liu, Q. Lei, *Sci. Rep.* **2016**, *6*, 33508.
[24] A. Altomare, M. Bozorg, K. Loos, in *Fascinating Fluoropolymers and Their Applications*. Progress in Fluorine Science (Eds: B. Ameduri, S. Fomin), Elsevier, Oxford **2020**, p. 45.
[25] F. Fang, W. Yang, C. Jia, X. Luo, *Appl. Phys. Lett.* **2008**, *92*, 222906.
[26] W. Xia, J. Zhou, T. Hu, P. Ren, G. Zhu, Y. Yin, J. Li, Z. Zhang, *Composites, Part A* **2020**, *131*, 105805.
[27] S. Filipović, V. P. Pavlović, M. Mitrić, S. Lević, N. Mitrović, A. Maričić, B. Vlahović, V. B. Pavlović, *J. Adv. Ceram.* **2019**, *8*, 133.
[28] J. G. Petrović, D. I. Olćan, N. N. Obradović, A. R. Djordjević, *IEEE Trans. Microwave Theory Tech.* **2022**, *70*, 970.
[29] W.-S. Cho, E. Hamada, *J. Alloys Compd.* **1998**, *266*, 118.
[30] L. Kilanski, S. Lewinska, A. Slawska-Waniewska, V. B. Pavlović, S. Filipović, *Inorg. Chem. Commun.* **2022**, *145*, 109960.
[31] A. Lassoued, B. Dkhil, A. Gadri, S. Ammar, *Results Phys.* **2017**, *7*, 3007.
[32] S. F. Mendes, C. M. Costa, C. Caparros, V. Sencadas, S. Lanceros-Méndez, *J. Mater. Sci.* **2012**, *47*, 1378.
[33] D. Okada, H. Kaneko, K. Kato, S. Furumi, M. Takeguchi, Y. Yamamoto, *Macromolecules* **2015**, *48*, 2570.
[34] R. Gregorio Jr., M. Cestari, *J. Polym. Sci., Part B: Polym. Phys.* **1994**, *32*, 859.
[35] Y. Jiang, Z. Zhang, Z. Zhou, H. Yang, Q. Zhang, *Polymers* **2019**, *11*, 1541.
[36] H. Abdolmaleki, S. Agarwala, *Polymers* **2020**, *12*, 2430.
[37] S. K. Rath, S. Dubey, G. S. Kumar, S. Kumar, A. K. Patra, J. Bahadur, A. K. Singh, G. Harikrishnan, T. U. Patro, *J. Mater. Sci.* **2014**, *49*, 103.
[38] T. U. Patro, M. V. Mhalgi, D. V. Khakhar, A. Misra, *Polymer* **2008**, *49*, 3486.
[39] G. Mago, F. T. Fisher, D. M. Kalyon, *J. Nanosci. Nanotechnol.* **2009**, *9*, 3330.
[40] B. Mohammadi, A. A. Yousefi, S. M. Bellah, *Polym. Test.* **2007**, *26*, 42.
[41] W. Ma, J. Zhang, S. Chen, X. Wang, *J. Macromol. Sci., Part B: Phys.* **2008**, *47*, 434.
[42] O. D. Jayakumar, E. H. Abdelhamid, V. Kotari, B. P. Mandal, R. Rao, Jagannath, V. M. Naik, R. Naik, A. K. Tyagi, *Dalton Transactions* **2015**, *44*, 15872.
[43] M. M. Rahman, F. Fabregat, A. Guerrero, A. M. Asiri, J. Bisquert, *ChemistrySelect* **2018**, *3*, 12169.
[44] H. Wang, H. Xie, S. Wang, Z. Gao, C. Li, G.-H. Hu, C. Xiong, *Composites, Part A* **2018**, *108*, 62.
[45] Q. Li, P. Peng, G.-X. Chen, S. W. Yoon, *J. Mater. Chem. C* **2014**, *2*, 8216.
[46] Z.-M. Dang, H.-Y. Wang, Y.-H. Zhang, J.-Q. Qi, *Macromol. Rapid Commun.* **2005**, *26*, 1185.

SUPPORTING INFORMATION

Additional supporting information can be found online in the Supporting Information section at the end of this article.

How to cite this article: S. Filipović, N. Obradović, C. Corlett, W. G. Fahrenholtz, M. Rosenschon, E. Füglein, R. Dojčilović, D. Tošić, J. Petrović, A. Đorđević, B. Vlahović, V. B. Pavlović, *J. Appl. Polym. Sci.* **2024**, *141*(10), e55040. https://doi.org/10.1002/app.55040